A Low Complexity PMI Selection Scheme for 3GPP 5G NR FDD Systems

Chun-Chia Tsai, Ting-Yu Yeh, Wei-Hung Chou, Wei-Chen Pao, and *Jen-Yi Pan
Industrial Technology Research Institute, Taiwan (R.O.C.)
*National Chung Cheng University, Taiwan (R.O.C.)
Email: cctsai60030@itri.org.tw; tingyuyeh@itri.org.tw; AlexChou@itri.org.tw; WCPao@itri.org.tw; *jypan@ccu.edu.tw

***Abstract*—In the 3rd generation partnership project (3GPP) new radio (NR) system, two types of codebooks, namely type I and type II, have been designed. Both types are utilized in the frequency division duplexed (FDD) codebook-based system. In the FDD codebook based system, the mobile station (MS) estimates channel state information (CSI) which includes the rank indicator (RI), the precoding matrix indicator (PMI), and the channel quality indicator (CQI), and feedbacks the CSI to the base station (BS). Although the type II CSI feedback promises more significant performance gain than the type I CSI feedback, the computational burden to estimate CSI is increased due to the high resolution of the type II codebook. This paper proposes a low complexity PMI selection scheme of type II codebook for 3GPP 5G NR FDD systems. The proposed scheme achieves similar performance to the conventional search scheme with a full search while the computational complexity is significantly reduced.**

***Index Terms*—5G NR, RI, PMI, type II codebook, system-level simulation**

I. Introduction

In 5G new radio (NR) systems, multiple-input multiple-output (MIMO) transmission is a key technique to improve the signal quality and the bandwidth efficiency of a wireless communication system. In the 3rd generation partnership project (3GPP) NR Release 15, two types of codebooks, namely type I and type II, have been specified for downlink (DL) precoding [1]. The two types of codebooks have different complexity and performance [2, 3]. The type I codebook has low resolution and low channel state information (CSI) feedback overhead, while the type II codebook has high resolution and high CSI feedback overhead [2, 3]. Although the type II codebook has higher CSI feedback overhead than the type I codebook, the type II CSI feedback owns superior performance gain to the type I CSI feedback [2, 3].

Both types of codebooks are utilized in the frequency division duplexed (FDD) codebook-based system. The codebook-based transmission is implemented in NR [1], while the actual advantages of MIMO would rely on the accurate CSI at the transmitter. For the NR FDD codebook-based system, the base station (BS) gets the downlink CSI by the mobile station (MS) feedback according to the predefined operations [4]. However, the conventional CSI search scheme is a linear searching [5] with the computations of the estimated channel on the MS side and the candidate precoding matrix. A full search is required. The searching space of the conventional codebook search scheme for precoding matrix indicator (PMI) search of type II codebook is huge because of the high resolution of the type II codebook [5]. Moreover, it would cause great power consumption in the MS as well.

In this paper, we propose a low complexity PMI selection scheme based on the singular value decomposition (SVD) scheme. According to WiSE system-level simulation [6, 7], the proposed scheme achieves similar performance to the conventional search scheme and reduces the computational complexity significantly. In addition, the proposed scheme still provides better performance gain than the type I conventional codebook search.

The remainder of this paper is organized as follows. In section II, we give an overview of Release 15 NR type I and type II codebooks. In section III, the proposed low complexity scheme is described in detail. In section IV, we analyze the complexity of the proposed scheme and the conventional scheme of type II codebook PMI selection. In section V, we present simulation results to demonstrate the efficiency of the proposed scheme. Finally, we draw our conclusions in section VI.

II. System Model

The precoding matrix $\boldsymbol{W}$ can be described as a product of two matrices $\boldsymbol{W_1}$ and $\boldsymbol{W_2}$ [2]:

$$\boldsymbol{W} = \boldsymbol{W_1}\, \boldsymbol{W_2} \tag{1}$$

where $\boldsymbol{W_1}$ targets wideband (WB) and long term channel properties. $\boldsymbol{W_2}$ targets frequency selective and short term channel properties. This section gives an overview of Release 15 NR type I and type II codebooks [1, 2, 8]. Both types are composed of 2D discrete Fourier transform (DFT) based grid of beams and enable the CSI feedback for beam selection and PSK based co-phase combining between two polarizations.

A. Type I Single Panel Codebook

The type I single panel precoding matrices $\boldsymbol{W}$ can be expressed as the two matrices $\boldsymbol{W_1}$ and $\boldsymbol{W_2}$.

$$\boldsymbol{W}_1 = \begin{pmatrix} \boldsymbol{X}_1 \otimes \boldsymbol{X}_2 & 0 \\ 0 & \boldsymbol{X}_1 \otimes \boldsymbol{X}_2 \end{pmatrix} \tag{2}$$

$\boldsymbol{W_2}$ performs beam selection and QPSK co-phasing between two polarizations.

$\boldsymbol{X}_1$ is an N_1 by L_1 matrix with L_1 column vectors $\boldsymbol{v}_h$ being an N_1O_1 oversampled DFT vector:

$$\boldsymbol{v}_h = \begin{bmatrix} 1 & e^{\frac{j2\pi h}{N_1 O_1}} & \dots & e^{\frac{j2\pi (N_1-1) h}{N_1 O_1}} \end{bmatrix} \tag{3}$$

$\boldsymbol{X}_2$ is an N_2 by L_2 matrix with L_2 column vectors $\boldsymbol{v}_u$ being an N_2O_2 oversampled DFT vector:

$$\boldsymbol{v}_u = \left[1 \quad e^{\frac{j2\pi u}{N_2O_2}} \quad \ldots \quad e^{\frac{j2\pi(N_2-1)u}{N_2O_2}}\right] \tag{4}$$

$\boldsymbol{X}_1 \otimes \boldsymbol{X}_2$ is a N_1N_2 by L_1L_2 matrix:

$$\boldsymbol{v}_{h,u,r} = \left[\boldsymbol{v}_u \quad e^{\frac{j2\pi h}{N_1O_1}}\boldsymbol{v}_u \quad \ldots \quad e^{\frac{j2\pi(N_1-1)h}{N_1O_1}}\boldsymbol{v}_u\right]^T \tag{5}$$

$L_1L_2 = L$. L is configurable: $L \in \{1, 4\}$[2]. N_1 and N_2 are the numbers of antenna ports in horizontal and vertical domains. O_1 and O_2 are the oversampling factors in both dimensions. h and u are horizontal and vertical beam indices. r is the polarization. The number of channel state information reference signal (CSI-RS) ports, $P_{CSI\text{-}RS}$, is $2N_1N_2$. TABLE I shows the number of CSI-RS antenna ports for type I and type II single panel codebook [1].

TABLE I. THE NUMBER OF CSI-RS ANTENNA PORTS FOR TYPE I AND TYPE II SINGLE PANEL CODEBOOK

Number of CSI-RS antenna ports, $P_{CSI\text{-}RS}$	(N_1, N_2)	(O_1, O_2)
4	(2, 1)	(4, 1)
8	(2, 2) (4, 1)	(4, 4) (4, 1)
12	(3, 2) (6, 1)	(4, 4) (4, 1)
16	(4, 2) (8, 1)	(4, 4) (4, 1)
24	(4, 3) (6, 2) (12, 1)	(4, 4) (4, 1)
32	(4, 4) (8, 2) (16, 1)	(4, 4) (4, 1)

B. Type II Single Panel Codebook

Type II single panel codebook supports rank 1 and rank 2, respectively. The codebook matrices $\boldsymbol{W}$ of rank 1 and rank 2 [2] are represented as:

For rank 1:
$$\boldsymbol{W} = \begin{bmatrix}\widetilde{\boldsymbol{w}}_{0,0} \\ \widetilde{\boldsymbol{w}}_{1,0}\end{bmatrix} \tag{6}$$

For rank 2:
$$\boldsymbol{W} = \begin{bmatrix}\widetilde{\boldsymbol{w}}_{0,0} & \widetilde{\boldsymbol{w}}_{0,1} \\ \widetilde{\boldsymbol{w}}_{1,0} & \widetilde{\boldsymbol{w}}_{1,1}\end{bmatrix} \tag{7}$$

$\widetilde{\boldsymbol{w}}_{r,l}$ is a weighted linear combination of L orthogonal beams per polarization r and rank l as:

$$\widetilde{\boldsymbol{w}}_{r,l} = \sum_{i=0}^{L-1} \boldsymbol{v}_{k_1^{(i)},k_2^{(i)},r} \cdot p_{r,l,i}^{(WB)} \cdot p_{r,l,i}^{(SB)} \cdot c_{r,l,i} \tag{8}$$

where $\boldsymbol{v}_{k_1^{(i)},k_2^{(i)},r}$ is an over sampled wideband 2D DFT beam.

$$k_1^{(i)} = O_1 \cdot n_1^{(i)} + q_1 \tag{9}$$

$$k_2^{(i)} = O_2 \cdot n_2^{(i)} + q_2 \tag{10}$$

$$q_1 = 0, \ldots, N_1 - 1, n_1^{(i)} = 0, \ldots, O_1 - 1 \tag{11}$$

$$q_2 = 0, \ldots, N_2 - 1, n_2^{(i)} = 0, \ldots, O_2 - 1 \tag{12}$$

The value of L is configurable: $L \in \{2, 3, 4\}$[1, 2], and $p_{r,l,i}^{(WB)}$ is the wideband beam amplitude scaling factor set mapping [1] as seen in TABLE II, which independently selected for each beam i and polarization r and rank l [2]. $p_{r,l,i}^{(SB)}$ is the sub-band (SB) beam amplitude scaling factor set mapping [1] as seen in TABLE III, which independently selected for each beam i and polarization r and rank l [2]. $c_{r,l,i}$ is the sub-band beam combining coefficient independently selected for each beam i and polarization r and rank l [2]. The phase combining coefficient is QPSK or 8PSK [1].

TABLE II. WIDEBAND BEAM AMPLITUDE SCALING FACTOR INDICES MAPPING

Indices	0	1	2	3	4	5	6	7
$p_{r,l,i}^{(WB)}$	0	$\sqrt{\frac{1}{64}}$	$\sqrt{\frac{1}{32}}$	$\sqrt{\frac{1}{16}}$	$\sqrt{\frac{1}{8}}$	$\sqrt{\frac{1}{4}}$	$\sqrt{\frac{1}{2}}$	1

TABLE III. SUB-BAND BEAM AMPLITUDE SCALING FACTOR INDICES MAPPING

Indices	0	1
$p_{r,l,i}^{(SB)}$	0	$\sqrt{\frac{1}{2}}$

III. PROPOSED LOW COMPLEXITY SCHEME

The search space for PMI search is huge when a full search is implemented, especially in the type II codebook. Due to the implementation difficulty, we propose a scheme to reduce the search complexity of the type II codebook PMI. The design principle is to perform SVD on the estimated channel to obtain the channel eigenvector. The channel eigenvector is taken as the ideal codebook accordingly. The inner product of the ideal codebook and the candidate DFT beams is operated to find the maximum amplitude value from the inner product results. The maximum orthogonal DFT beam is applied to quantify the type II codebook PMI. The flow chart of the proposed scheme is shown in Fig. 1.

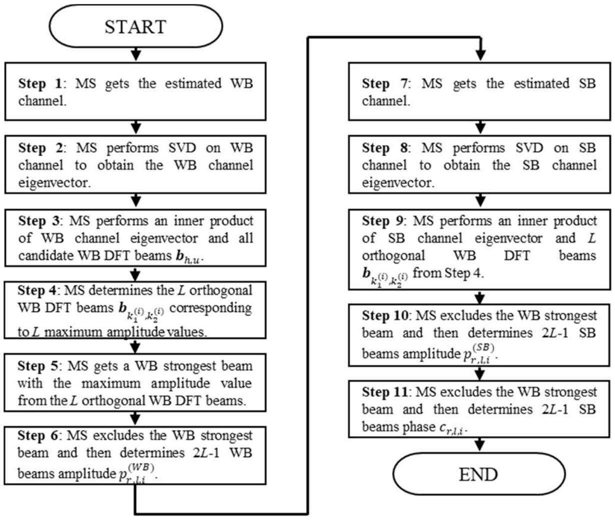

Fig. 1. The flow chart of proposed scheme.

The steps of the proposed scheme are as follows:

Step 1: The MS uses the non-precoded CSI-RS to estimate the wideband downlink channel $\widehat{\boldsymbol{H}}^{(WB)}$.

Step 2: The MS performs SVD on the wideband channel and gets the wideband channel eigenvector $\boldsymbol{V}_l^{(WB)}$,

$$\widehat{\boldsymbol{H}}^{(WB)} = \boldsymbol{U}^{(WB)}\boldsymbol{\Sigma}^{(WB)}\boldsymbol{V}_l^{H(WB)} \tag{13}$$

where $\widehat{\boldsymbol{H}}^{(WB)}$ is the estimated wideband channel. $\boldsymbol{U}^{(WB)}$ and $\boldsymbol{V}_l^{H(WB)}$ are the unitary matrices. $\boldsymbol{\Sigma}^{(WB)}$ is the rectangular diagonal matrix. l is the rank.

Step 3: The MS performs an inner product of wideband channel eigenvector and all candidate wideband DFT beams $\boldsymbol{b}_{h,u} = \begin{bmatrix}\boldsymbol{v}_{h,u,0}\\ \boldsymbol{v}_{h,u,1}\end{bmatrix}$ within the beam group,

$$\begin{aligned}
&\mathrm{dot}\left(\boldsymbol{V}_l^{(WB)}, \boldsymbol{b}_{h,u}\right)\\
&= \mathrm{dot}\left(\begin{bmatrix}\boldsymbol{V}_{0,l}^{(WB)}\\ \boldsymbol{V}_{1,l}^{(WB)}\end{bmatrix}, \begin{bmatrix}\boldsymbol{v}_{h,u,0}\\ \boldsymbol{v}_{h,u,1}\end{bmatrix}\right)\\
&= \begin{bmatrix}\boldsymbol{V}_{0,l}^{H(WB)} & \boldsymbol{V}_{1,l}^{H(WB)}\end{bmatrix}\begin{bmatrix}\boldsymbol{v}_{h,u,0}\\ \boldsymbol{v}_{h,u,1}\end{bmatrix}\\
&= \boldsymbol{V}_{0,l}^{H(WB)}\boldsymbol{v}_{h,u,0} + \boldsymbol{V}_{1,l}^{H(WB)}\boldsymbol{v}_{h,u,1}\\
&= \beta_{h,u,0,l}^{(WB)} + \beta_{h,u,1,l}^{(WB)}\\
&= A_{h,u,0,l}^{(WB)} e^{j\varphi_{h,u,0,l}^{(WB)}} + A_{h,u,1,l}^{(WB)} e^{j\varphi_{h,u,1,l}^{(WB)}}\\
&= \textstyle\sum_{r=0}^{1} A_{h,u,r,l}^{(WB)} e^{j\varphi_{h,u,r,l}^{(WB)}}
\end{aligned} \tag{14}$$

where $A_{h,u,r,l}^{(WB)}$ is the wideband amplitude and $\varphi_{h,u,r,l}^{(WB)}$ is the wideband phase angle. h and u are horizontal and vertical beam indices respectively. r is the polarization and l is the rank.

Step 4: The MS gets the L orthogonal wideband DFT beams $\boldsymbol{b}_{k_1^{(i)},k_2^{(i)}}$ corresponding to L maximum amplitude values after performing the inner product.

$$A_{k_1^{(i)},k_2^{(i)},l}^{(WB)} = \max_{h,u}\left(\textstyle\sum_{r=0}^{1} A_{h,u,r,l}^{(WB)}\right), i = 0, \dots, L-1 \tag{15}$$

Step 5: The MS sorts the L wideband DFT beams $\boldsymbol{v}_{k_1^{(i)},k_2^{(i)},0}$ and the corresponding polarization beams $\boldsymbol{v}_{k_1^{(i)},k_2^{(i)},1}$ to get a wideband strongest beam with the maximum amplitude value,

$$A_{k_1^{(s)},k_2^{(s)},r,l}^{(WB)} = \max_i A_{k_1^{(i)},k_2^{(i)},r,l}^{(WB)}, i = 0, \dots, L-1 \tag{16}$$

where $A_{k_1^{(s)},k_2^{(s)},r,l}^{(WB)}$ is the wideband strongest beam amplitude. $s \in \{0, \dots, L-1\}$.

Step 6: The MS excludes the wideband strongest beam $\boldsymbol{v}_{k_1^{(s)},k_2^{(s)},r}$ and then determines 2L-1 remaining wideband beams amplitude $p_{r,l,i}^{(WB)}$ based on a normalization function and a mapping wideband amplitude table.

$$\begin{bmatrix} p_{0,l,0}^{(WB)}\\ \vdots\\ p_{0,l,L-1}^{(WB)}\\ p_{1,l,0}^{(WB)}\\ \vdots\\ p_{1,l,L-1}^{(WB)} \end{bmatrix} = \begin{bmatrix} A_{k_1^{(0)},k_2^{(0)},0,l}^{(WB)} / A_{k_1^{(s)},k_2^{(s)},r,l}^{(WB)}\\ \vdots\\ A_{k_1^{(L-1)},k_2^{(L-1)},0,l}^{(WB)} / A_{k_1^{(s)},k_2^{(s)},r,l}^{(WB)}\\ A_{k_1^{(0)},k_2^{(0)},1,l}^{(WB)} / A_{k_1^{(s)},k_2^{(s)},r,l}^{(WB)}\\ \vdots\\ A_{k_1^{(L-1)},k_2^{(L-1)},1,l}^{(WB)} / A_{k_1^{(s)},k_2^{(s)},r,l}^{(WB)} \end{bmatrix}, l = 0,1 \tag{17}$$

Step 7: The MS uses the non-precoded CSI-RS to estimate the sub-band downlink channel $\widehat{\boldsymbol{H}}^{(SB)}$.

Step 8: The MS performs SVD on the sub-band channel and gets the sub-band channel eigenvector $\boldsymbol{V}_l^{(SB)}$,

$$\widehat{\boldsymbol{H}}^{(SB)} = \boldsymbol{U}^{(SB)}\boldsymbol{\Sigma}^{(SB)}\boldsymbol{V}_l^{H(SB)} \tag{18}$$

where $\widehat{\boldsymbol{H}}^{(SB)}$ is the estimated sub-band channel. $\boldsymbol{U}^{(SB)}$ and $\boldsymbol{V}_l^{H(SB)}$ are the unitary matrices, and $\boldsymbol{\Sigma}^{(SB)}$ is the rectangular diagonal matrix.

Step 9: The MS performs an inner product of sub-band channel eigenvector and L orthogonal wideband DFT beams $\boldsymbol{b}_{k_1^{(i)},k_2^{(i)}} = \begin{bmatrix}\boldsymbol{v}_{k_1^{(i)},k_2^{(i)},0}\\ \boldsymbol{v}_{k_1^{(i)},k_2^{(i)},1}\end{bmatrix}$ from Step 4.

$$\begin{aligned}
&\mathrm{dot}\left(\boldsymbol{V}_l^{(SB)}, \boldsymbol{b}_{k_1^{(i)},k_2^{(i)}}\right) \\
&= \mathrm{dot}\left(\begin{bmatrix}\boldsymbol{V}_{0,l}^{(SB)} \\ \boldsymbol{V}_{1,l}^{(SB)}\end{bmatrix}, \begin{bmatrix}\boldsymbol{v}_{k_1^{(i)},k_2^{(i)},0} \\ \boldsymbol{v}_{k_1^{(i)},k_2^{(i)},1}\end{bmatrix}\right) \\
&= \begin{bmatrix}\boldsymbol{V}_{0,l}^{H(SB)} & \boldsymbol{V}_{1,l}^{H(SB)}\end{bmatrix}\begin{bmatrix}\boldsymbol{v}_{k_1^{(i)},k_2^{(i)},0} \\ \boldsymbol{v}_{k_1^{(i)},k_2^{(i)},1}\end{bmatrix} \\
&= \boldsymbol{V}_{0,l}^{H(SB)}\boldsymbol{v}_{k_1^{(i)},k_2^{(i)},0} + \boldsymbol{V}_{1,l}^{H(SB)}\boldsymbol{v}_{k_1^{(i)},k_2^{(i)},1} \\
&= \beta_{k_1^{(i)},k_2^{(i)},0,l}^{(SB)} + \beta_{k_1^{(i)},k_2^{(i)},1,l}^{(SB)} \\
&= A_{k_1^{(i)},k_2^{(i)},0,l}^{(SB)} e^{j\varphi_{k_1^{(i)},k_2^{(i)},0,l}^{(SB)}} + A_{k_1^{(i)},k_2^{(i)},1,l}^{(SB)} e^{j\varphi_{k_1^{(i)},k_2^{(i)},1,l}^{(SB)}} \\
&= \sum_{r=0}^{1} A_{k_1^{(i)},k_2^{(i)},r,l}^{(SB)} e^{j\varphi_{k_1^{(i)},k_2^{(i)},r,l}^{(SB)}} \qquad (19)
\end{aligned}$$

where $A_{k_1^{(i)},k_2^{(i)},r,l}^{(SB)}$ is the sub-band amplitude and $\varphi_{k_1^{(i)},k_2^{(i)},r,l}^{(SB)}$ is the sub-band phase angle.

Step 10: The MS excludes the wideband strongest beam $\boldsymbol{v}_{k_1^{(s)},k_2^{(s)},r}$ and then determines 2*L*-1 remaining sub-band beams amplitude $p_{r,l,i}^{(SB)}$ based on a normalization function and a mapping sub-band amplitude table.

$$\begin{bmatrix} p_{0,l,0}^{(SB)} \\ \vdots \\ p_{0,l,L-1}^{(SB)} \\ p_{1,l,0}^{(SB)} \\ \vdots \\ p_{1,l,L-1}^{(SB)} \end{bmatrix} = \begin{bmatrix} A_{k_1^{(0)},k_2^{(0)},0,l}^{(SB)} / A_{k_1^{(s)},k_2^{(s)},r,l}^{(WB)} \\ \vdots \\ A_{k_1^{(L-1)},k_2^{(L-1)},0,l}^{(SB)} / A_{k_1^{(s)},k_2^{(s)},r,l}^{(WB)} \\ A_{k_1^{(0)},k_2^{(0)},1,l}^{(SB)} / A_{k_1^{(s)},k_2^{(s)},r,l}^{(WB)} \\ \vdots \\ A_{k_1^{(L-1)},k_2^{(L-1)},1,l}^{(SB)} / A_{k_1^{(s)},k_2^{(s)},r,l}^{(WB)} \end{bmatrix}, l = 0,1 \qquad (20)$$

Step 11: The MS excludes the wideband strongest beam $\boldsymbol{v}_{k_1^{(s)},k_2^{(s)},r}$ and then determines 2*L*-1 remaining sub-band beams phase $c_{r,l,i}$ based on a mapping sub-band phase table.

$$\begin{bmatrix} c_{0,l,0} \\ \vdots \\ c_{0,l,L-1} \\ c_{1,l,0} \\ \vdots \\ c_{1,l,L-1} \end{bmatrix} = \begin{bmatrix} \varphi_{k_1^{(0)},k_2^{(0)},0,l}^{(SB)} \\ \vdots \\ \varphi_{k_1^{(L-1)},k_2^{(L-1)},0,l}^{(SB)} \\ \varphi_{k_1^{(0)},k_2^{(0)},1,l}^{(SB)} \\ \vdots \\ \varphi_{k_1^{(L-1)},k_2^{(L-1)},1,l}^{(SB)} \end{bmatrix}, l = 0,1 \qquad (21)$$

With the steps of the proposed scheme, MS can quickly determine the type II codebook PMI.

IV. Computational Complexity Comparison

In this section, we compare the complexity of the proposed scheme with the conventional scheme. The comparison method is to calculate the overhead required for the MS to search the type II codebook PMI. We take the number of bits as a quantized operation for example.

TABLE IV. Example Payload Calculation for Conventional Scheme

	Rank 1 conventional scheme (bits)	Rank 2 conventional scheme (bits)
Rotation $\lceil \log_2(O_1O_2) \rceil$	2	2
***L* beam selection ($log_2\binom{N_1N_2}{L}$)**	0	0
Strongest coefficient $\lceil \log_2 2L \rceil$ per rank	2	4
WB amplitude $3 \times (2L-1)$ per rank	9	18
SB amplitude (1 SB) $1 \times (K-1)$ per rank	0	0
SB phase (1 SB) $3 \times (K-1) +$ $2 \times (2L-K)$ per rank	9	18
Total (WB + 1SB)	22	42

(*) Note: *K*=4, 4, and 6 for *L*=2, 3, and 4, respectively

We can see an example payload calculation from TABLE IV and TABLE V for the conventional scheme and the proposed scheme, respectively. Release 15 type II CSI at $L = 2$, 8PSK phase quantization and 4 ports (N_1, N_2, O_1, O_2) = (2, 1, 4, 1) with wideband amplitude requires a modulo operation.

TABLE V. Example Payload Calculation for Proposed Scheme

	Rank 1 proposed scheme (bits)	Rank 2 proposed scheme (bits)
Rotation $\lceil \log_2(O_1O_2) \rceil$	2	2
***L* beam selection ($log_2\binom{N_1N_2}{L}$)**	0	0
Strongest coefficient per rank	2	3
WB amplitude per rank	≈ 5	≈ 6
SB amplitude (1 SB) per rank	0	0
SB phase (1 SB) per rank	≈ 5	≈ 6
Total (WB + 1SB)	≈ 7	≈ 8

In TABLE IV, the PMI search complexity is $O(2^{22})$ and $O(2^{42})$ for rank 1 and 2. In TABLE V, it can be observed that the PMI search complexity is around $O(2^{7})$ and $O(2^{8})$ for rank 1 and 2. Without a need of a linear search to try all the indices of type II codebook, the proposed scheme uses the SVD operation to find the maximum orthogonal DFT beams and to determine the strongest coefficient, the wideband amplitude $p_{r,l,i}^{(WB)}$, the sub-band amplitude $p_{r,l,i}^{(SB)}$, and the sub-band phase $c_{r,l,i}$. Obviously, the MS implementation complexity is greatly reduced, especially at rank 2.

V. Simulation Results

We present simulation results via the WiSE simulator [7]. TABLE VI shows the parameters for indoor - eMBB 12 TRxP. Model A [9]. Fig. 2 and Fig. 3 show the CDF of the channel capacity by testing CSI feedback 1000 times.

In Fig. 2, the performance of the proposed scheme of type II QPSK is similar to that of the conventional scheme of type II QPSK. Only around 2% performance loss is observed. Nevertheless, the simulation execution time of the proposed scheme is significantly reduced. The conventional scheme takes 866.5 seconds, while the proposed scheme only takes 0.02 seconds. In addition, the proposed scheme of type II codebook outperforms the conventional scheme of type I codebook. Around 8% performance gain is observed.

In Fig. 3, the performance of the proposed scheme of type II 8PSK is similar to that of the conventional scheme of type II 8PSK. Similarly, around 2% performance loss is observed, but the execution time is significantly reduced. The conventional scheme takes 7275.97 seconds, while the proposed scheme only takes 0.03 seconds. The proposed scheme of type II codebook still outperforms the conventional scheme of type I codebook. More than 9% performance gain is observed.

TABLE VI. Simulation Assumption for Indoor-eMBB

Parameter	Value
Carrier frequency	4 GHz
BS antenna height	3 m
Total transmit power per TRP	21 dBm for 10 MHz bandwidth
MS power class	23 dBm
Inter site distance	20 m
TRP antenna configuration	(*M, N, P, Mg, Ng; Mp, Np*) = (4, 4, 2, 1, 1; 2, 1) for 4 ports; (*M, N, P, Mg, Ng; Mp, Np*) = (4, 4, 2, 1, 1; 4, 2) for 16 ports; (*M, N, P, Mg, Ng; Mp, Np*) = (4, 4, 2, 1, 1; 4, 4) for 32 ports;
MS antenna configuration	(*M, N, P, Mg, Ng; Mp, Np*) = (1, 2, 2, 1, 1; 1, 1) for 1 port;
Antenna element gain	5 dBi for BS; 0 dBi for MS
MS speeds	100% indoor, 3 km/h
Noise figure	5 dB for BS; 7 dB for MS
Traffic model	Full buffer
MS density	10 MSs per TRxP, randomly and uniformly dropped throughout the geographical area
Channel model	InH_A

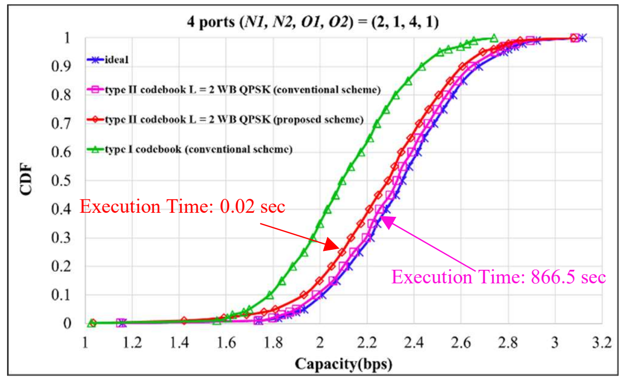

Fig. 2. Comparison of channel capacity between the proposed scheme and the conventional scheme of type II QPSK.

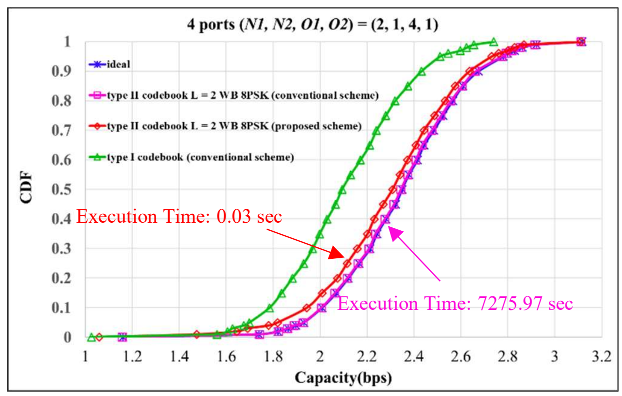

Fig. 3. Comparison of channel capacity between the proposed scheme and the conventional scheme of type II 8PSK.

The average spectral efficiency and the 5th percentile user spectral efficiency are shown in TABLE VII and TABLE VIII for 16 and 32 ports, respectively. System-level simulation evaluation methodologies are defined [10]. In TABLE VII, the values of the average spectral efficiency and the 5th percentile user spectral efficiency of the conventional scheme of type I codebook are 7.31057 bps/Hz and 0.201394 bps/Hz. The values of the average spectral efficiency and the 5th percentile user spectral efficiency of the proposed scheme of type II codebook are 7.41185 bps/Hz and 0.235819 bps/Hz. Comparing the proposed scheme of type II codebook with the conventional scheme of type I codebook, the proposed scheme of type II codebook has the 1.385% gain in average spectral efficiency, and the proposed scheme of type II codebook has the 17.09% gain in the 5th percentile user spectral efficiency.

In TABLE VIII, the values of the average spectral efficiency and the 5th percentile user spectral efficiency of the conventional scheme of type I codebook are 8.03267 bps/Hz and 0.257215 bps/Hz. The values of the average spectral efficiency and the 5th percentile user spectral efficiency of the proposed scheme of type II codebook are 8.10049 bps/Hz and 0.321024 bps/Hz. Comparing the proposed scheme of type II codebook with the conventional scheme of type I codebook, the proposed scheme of type II codebook has the 0.844% gain in average spectral efficiency, and the proposed scheme of type II codebook has the 24.808% gain in the 5th percentile user spectral efficiency.

The WiSE system-level simulation results show that the proposed scheme of type II codebook outperforms the conventional scheme of type I codebook, especially in the 5th percentile user spectral efficiency.

TABLE VII. COMPARISION OF SPECTRAL EFFICIENCY IN SYSTEM LEVEL SIMULATION ANTENNA CONFIGURATION 16 PORTS $(N_1, N_2, O_1, O_2) = (4, 2, 4, 4)$

Codebook	DL average spectral efficiency(bps/Hz)	DL 5th percentile user spectral efficiency(bps/Hz)
Type I (conventional scheme)	7.31057	0.201394
Type II (proposed scheme)	7.41185	0.235819

TABLE VIII. COMPARISION OF SPECTRAL EFFICIENCY IN SYSTEM LEVEL SIMULATION ANTENNA CONFIGURATION 32 PORTS $(N_1, N_2, O_1, O_2) = (4, 4, 4, 4)$

Codebook	DL average spectral efficiency(bps/Hz)	DL 5th percentile user spectral efficiency(bps/Hz)
Type I (conventional scheme)	8.03267	0.257215
Type II (proposed scheme)	8.10049	0.321024

VI. CONCLUSION

This paper proposes a low complexity PMI selection scheme of type II codebook for 3GPP 5G NR FDD systems. Compared to the conventional search scheme, the proposed scheme achieves a very low computational complexity while maintaining comparable performance. The proposed scheme is very suitable and feasible for the implementation in 3GPP 5G NR FDD systems.

ACKNOWLEDGMENT

This work was supported in part by the Ministry of Science and Technology (MOST) of Taiwan under Grants MOST109-2218-E-194-007, MOST110-2221-E-194-020, and MOST110-2224-E-305-001 and in part by the Industrial Technology Research Institute (ITRI), Taiwan.

REFERENCES

[1] 3GPP Technical Specification (TS) 38.214 v15.8.0, "NR; Physical layer procedure for data (Release 15)," Dec. 2019.

[2] 3GPP R1-1709232, "WF on type I and II CSI codebooks," 3GPP TSG RAN WG1 Meeting #89, May 2017.

[3] E. Onggosanusi, M. S. Rahman, L. Guo, Y. Kwak, H. Noh, Y. Kim, S. Faxer, M. Harrison , M. Frenne, S. Grant, R. Chen, R. Tamrakar, and Q. Gao, "Modular and high-resolution channel state information and beam management for 5G New Radio, " *IEEE Commun. Mag.*, vol. 56, no. 3, pp. 48-55, Mar. 2018.

[4] 3GPP Technical Specification (TS) 36.213 v15.8.0, "E-UTRA; Physical layer procedures (Release 15)," Dec. 2019.

[5] 3GPP R1-1801809, "UE capability of type II codebook," 3GPP TSG RAN WG1 Meeting #92, Feb. 2018.

[6] COMMRESEARCH, https://www.commresearch.com.tw.

[7] C. K. Jao, C. Y. Wang, T. Y. Yeh, C. C. Tsai, L. C. Lo, J. H. Chen, W. C. Pao, W. H. Sheen, "WiSE: A system-level simulator for 5G mobile networks," *IEEE Wireless Communications*, vol. 25, no. 2, pp. 4-7, Apr. 2018.

[8] D. Erik, P. Stefan, S. Johan, 5G NR: The Next Generation Wireless Access Technology. , Academic Press, 2018.

[9] 3GPP RP-180524, "Summary of calibration results for IMT-2020 self evaluation," 3GPP TSG RAN Meeting #79, Mar. 2018.

[10] ITU-R Report ITU-R M.2412, "Guidelines for evaluation of radio interface technologies for IMT-2020," ITU-R WP 5D, Oct. 2017.